Hindawi
Shock and Vibration
Volume 2021, Article ID 1881870, 15 pages
https://doi.org/10.1155/2021/1881870

Research Article

Study on Combined Energy Absorption Support for Rockburst Disaster Control in Tunnelling

Liang Kuang[1,2], **Gang Wang**[3], **Wenge Qiu**[1], **Lun Gong**[1], **Zhiqiang Feng**[4] and **Tianhui Ma**[4]

[1]*Key Laboratory of Transportation Tunnel Engineering, Ministry of Education, Southwest Jiaotong University, Chengdu 610031, Sichuan, China*
[2]*China Railway Eryuan Engineering Group Co.Ltd, Chengdu 610031, Sichuan, China*
[3]*College of Transportation Engineering, Nanjing Tech University, Nanjing 210009, Jiangsu, China*
[4]*Institute of Rock Instability and Seismicity Research, Dalian University of Technology, Dalian 116024, Liaoning, China*

Correspondence should be addressed to Gang Wang; swjtu_wg@163.com

Received 21 September 2021; Revised 19 November 2021; Accepted 20 November 2021; Published 2 December 2021

Academic Editor: Chengwei Fei

In order to better realize the rockburst disaster control mechanism and approach, the rockburst response of concrete blocks with different energy absorption levels under different energy storage conditions was observed and analyzed by loading tests. The occurrence and control mechanism of rockburst were explored from the perspective of energy aggregation and energy dissipation. On this basis, a combined energy absorption support system of concrete-filled steel tube frames and hollow steel pipes for rockburst disaster control was designed, and the effectiveness of the system was verified by numerical simulation and field tests. The results of loading tests show that the failure mode of the specimens changes from static failure to dynamic burst under energy storage loading. The occurrence of rockburst is inevitable when the energy supply is sufficient, but the disaster can be reduced or eliminated by strengthening constraints and improving energy-absorbing capacity to transform rockburst into large deformation. The combined structure consists of the hollow steel pipes being energy-absorbing part and the concrete-filled steel tube frames being strong confinement part was proposed to control rockburst disaster in tunnel support. The numerical analysis on the dynamic response of the support under strong rockburst impact shows that the hollow steel pipes effectively reduced the impact force on the concrete-filled tube frames, and accordingly, the deformation of the entire support system decreased. Given the condition that the hollow steel pipes be able to absorb all the impact energy during deformation, the smaller the strength of the hollow steel pipe is, the smaller the impact force and the displacement is. The combined energy absorption support provides an effective solution for rockburst disaster management in tunnels with strict clearance requirements.

1. Introduction

With the increasing excavation depth of tunnels and mines, the frequency and damage degree of rockburst disasters increase sharply, which has a significant impact on the safety and stability of the project. Therefore, the occurrence and control mechanism of rockburst and effective control methods have been a key research topic in rock mechanics. In terms of rockburst research, indoor simulation experiment is an important link in the study of rockburst formation and control mechanism. Since the invention of rigid testing machine in 1966, the laboratory experiment for rockburst has developed rapidly, and it has also led to the discussion of rockburst mechanism. For example, Kidybinski [1] proposed to use the strain energy storage index to judge and predict rockburst through laboratory experiments. Pan et al. [2] developed a series of brittle failure equivalent materials according to the dynamic instability criterion of rockburst [3] and successfully carried out a chamber rockburst simulation experiment by self-made bidirectional loading device. Xu et al. [4] studied the effect of specimen thickness on rockburst test. Aliakbar Golshani

et al. [5] proposed the brittleness index related to rock brittleness before peak stress by studying the loading failure process of brittle rock. Zhou et al. [6] believed that plate cracking can be used as a precursor feature of rockburst and carried out a uniaxial compression plate cracking model test using high strength gypsum model specimens. He et al. [7] used the self-developed deep rockburst process experimental system to conduct experimental research on granite rockburst process under deep high stress conditions and obtained the whole process stress curve of granite rockburst by rapid unloading. Meng et al. [8] conducted shear tests under different normal stresses on fully closed granite joints formed by tension splitting. By analyzing the acoustic emission characteristics of rock, a method for predicting fault sliding rockburst caused by stress drop and stress drop based on acoustic emission b value was proposed. Shirani Faradonbeh et al. [9] summarized and analyzed a large number of rock true triaxial unloading experimental data and established the prediction model of rockburst maximum stress and its risk index. Scholars in related fields have explained the mechanism of rockburst from various angles. The relatively mature theories include strength theory, energy theory, stiffness theory, fracture mechanics, and damage theory [10–13]. At present, the most clear summary of the conditions for rockburst is that there is a high energy storage body, and its stress is close to the rock strength, which is the internal cause of rockburst, and the trigger of some additional loads is the external cause of rockburst [14, 15]. As mentioned above, laboratory experiments have greatly promoted the research on the mechanism of rockburst. However, up to now, there is no unified understanding of the formation mechanism of rockburst in the world [16, 17]. Therefore, it is still necessary to learn from the previous research results to improve the laboratory experimental facilities, specimens, and methods and further study the formation and control mechanism of rockburst.

Combined with the study of the control mechanism of rockburst, the treatment of rockburst in practical engineering has experienced a process from single flexible support or rigid support to the combination of flexible support and rigid support. Flexible support emphasizes the deformation ability of support components, while rigid support emphasizes the high strength performance, and their ability to absorb energy is limited. The key to controlling rockburst is to absorb the kinetic energy of rockburst, which requires both high strength and large deformation of supporting components. A variety of energy absorption structures have also been developed. At present, in the design of rockburst support means, measures can be taken to avoid or reduce the occurrence effect of rockburst in the static inoculation process, or to absorb the kinetic energy of ejection rock mass in the dynamic impact of rockburst to prevent the damage of ejection rock mass to construction personnel and machinery. The former is mainly composed of energy-absorbing bolts, steel mesh, and shotcrete [18], such as energy-absorbing bolts supporting rock mass in South Africa. In roadways where rockbursts occur frequently, Canada improves the stability of rock mass mainly through the combination of steel bolts and cone bolts with metal mesh. Steel fiber reinforced concrete, systematic bolts, and steel mesh were adopted to prevent rockburst in the diversion tunnel of Jinping II Hydropower Station [19]. The latter can use shotcrete to improve the integrity and strength of the surrounding rock surface, lay metal mesh to absorb the kinetic energy caused by rockburst, and intercept the flying rocks. It can also lay a flexible energy absorption cushion [20] between the surrounding rock and the steel arch to carry the rockfall load and absorb the kinetic energy of rockfall, so as to reduce the impact on the supporting system.

On the basis of previous laboratory rockburst experimental research, this paper will study the failure characteristics of specimens under different lateral constraints by self-developed indoor experimental device and further explore the control mechanism of rockburst. According to the experimental results, a combined energy absorption support system suitable for rockburst control is proposed, and the control effect of rockburst disaster is evaluated by numerical experiments of impact load.

2. Experiment on Rockburst Control Mechanism

2.1. Experimental Equipment. After the excavation of the engineering rock mass, the high stress makes the rock mass in the rockburst area accumulate certain elastic potential energy, which is different from the rigid loading in the laboratory. Therefore, in order to simulate the loading situation in practical engineering, the experiment adopts the originally developed uniaxial energy storage loading device, which is mainly composed of three parts: the counterforce frame, the Jack, and the energy storage loading device, as shown in Figures 1 and 2. The counterforce frame is composed of two homogeneous steel plates and four connecting columns with a size of $600\,\text{mm} \times 700\,\text{mm} \times 50\,\text{mm}$. The Jack diameter is 95 mm, the maximum stroke is 100 mm, and the maximum load is 200 kN. The pressure gage is used to read the jacking pressure during the process of the experiment. The energy storage loader is composed of a force transmission plate, five steel sleeves, five springs ($k = 400\,\text{kN/m}$), and a loading plate. The steel sleeve is welded on the loading plate, and the spring is placed in the steel sleeve to connect the upper force transmission plate and the lower loading plate. The height of the steel sleeve is designed as the spring compaction height. When the spring is compacted, the force transmission plate contacts with the steel sleeve.

The spring stiffness is obviously smaller than that of the concrete specimen, so the device can realize the spring compression energy storage in the loading process. When the specimen reaches the ultimate bearing capacity and fails, the material strength decreases instantaneously, the spring bounces back and releases elastic potential energy, which continuously provides impact energy for the failure of rockmass. Thus, the stress variation law and energy aggregation state of rock mass during rockburst are simulated. When the spring is removed, the transmission plate is placed directly on the steel sleeve, then the energy storage loading device is transformed into a rigid nonenergy storage loading device.

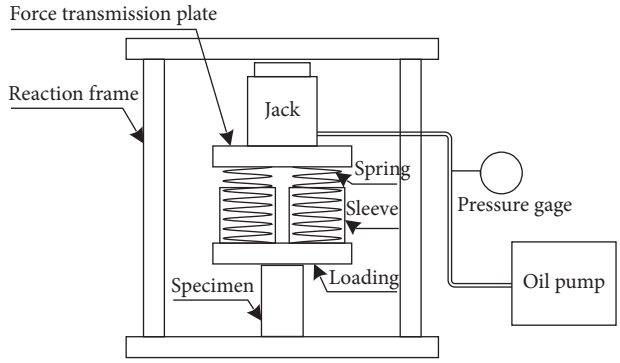

Figure 1: Design drawing of uniaxial energy storage loading device.

Figure 2: Field test diagram of uniaxial energy storage loading device.

2.2. Specimen Preparation. The specimens were divided into four types: cylindrical concrete specimen, composite-1 specimen (C-1), composite-2 specimen (C-2), and composite-3 specimen (C-3). The composite specimens were made by gradually increasing the lateral confinement of cylindrical concrete specimens.

2.2.1. Cylindrical Concrete Specimen. The designed strength grade of the concrete is C20. The constituents used to make the specimen include 5 to 10 mm gravel, composite silicate cement with the class of strength being 32.5 R, and machine-made sand with the modulus of fineness being 2.8. The mix proportion ratio of concrete adopts 1 (water): 1.43 (cement): 3.56 (fine aggregate): 4.01 (coarse aggregate).

The concrete was poured into a PVC pipe with an inner diameter of 60 mm, a wall thickness of 2.5 mm, and a height of 100 mm. After standard curing the concrete to the design strength age, the PVC pipe was cut and stripped to obtain a concrete cylinder block, as shown in Figure 3(a).

2.2.2. Composite-1 Specimen (C-1). The materials and manufacturing methods used in the C-1 specimen are the same as those used in the cylindrical concrete specimen. The difference is that the final step is not to strip all PVC pipes, but to cut only the PVC pipe of 10 mm length at the top to obtain the C-1 specimen, as shown in Figure 3(b). In this way, the PVC pipe can be close to and constraint the concrete specimen, while avoiding the axial force applied to the PVC pipe during the test.

2.2.3. Composite-2 Specimen (C-2). The C-2 specimen was obtained by tightly wrapping the C-1 specimen with a single galvanized iron wire with a diameter of 2.0 mm, as shown in Figure 3(c).

2.2.4. Composite-3 Specimen (C-3). By wrapping the C-2 specimen with a tight rubber ring with a wall thickness of 2.125 mm, the C-3 specimen was obtained, as shown in Figure 3(d).

2.3. Experimental Design. In this paper, the uniaxial loading tests of energy storage and nonenergy storage are carried out, respectively. The rockburst reactions of specimens with different energy absorption levels under different energy storage levels are observed and analyzed to explore the occurrence conditions and control methods of rockburst from the perspective of energy aggregation and energy dissipation. The specific experimental conditions are shown in Table 1.

2.4. Failure Characteristics of Specimens. The strength of rockburst or static failure can be judged by the macroscopic failure characteristics, such as the flying radius of fragments

(a) (b) (c) (d)

Figure 3: Concrete specimens under different constraints: (a) cylindrical concrete, (b) C-1, (c) C-2, (d) C-3.

Table 1: Test conditions.

Condition	Loading method	Specimen
1	Nonenergy storage, slow loading	Cylindrical concrete
2	Nonenergy storage, fast loading	Cylindrical concrete
3	Energy storage, slow loading	Cylindrical concrete
4	Energy storage, fast loading	Cylindrical concrete
5	Energy storage, slow loading	Cylindrical concrete + PVC pipe (C-1)
6	Energy storage, slow loading	Cylindrical concrete + PVC pipe + iron hoop (C-2)
7	Energy storage, slow loading	Cylindrical concrete + PVC pipe + iron hoop + rubber (C-3)

Note: The loading speed of slow loading is about 0.35 MPa·s^{-1} according to the "Standard for test method of mechanical properties on ordinary concrete" in China. The fast loading speed is 5 times that of slow loading.

and the maximum failure load. Table 2 lists the experimental results under various loading conditions.

From Figures 4(a) ~ 4(d), it can be seen that the failure mode of the specimens changed from static shear failure to dynamic impact failure under energy storage loading from condition 1 to condition 4. Nonaccumulative loading is a rigid loading of the specimen through the displacement of the Jack. The loading system cannot impose force on the specimen beyond its bearing capacity. The energy provided by the loading system is always equal to the energy consumed by the specimen, and the specimen will not explode. In the energy storage loading, the spring was compressed and stored before the specimen reached the peak bearing capacity. After the specimen reached the bearing capacity limit and was damaged, the spring bounced back quickly and continued to apply the force greater than its bearing capacity to the specimen to continuously and rapidly apply the accumulated energy to the specimen. As shown in Figure 5, the integrity of the block is damaged, and the residual energy absorption ability cannot consume this part of the energy. The static failure is transformed into dynamic failure, and the residual energy $\triangle$E of the external load is released in the form of kinetic energy. The concrete block flies out and bursts. Therefore, whether the rock mass can be given enough energy after reaching the ultimate bearing capacity determines whether the rockburst can occur. In addition, due to the incomplete coordination between specimen deformation and loading load, the speed of loading rate will affect the ultimate bearing capacity of rock mass and the energy accumulated during blasting.

The concrete specimen wrapped by PVC pipe can be regarded as a tension-compression coupling material. When the axial load is applied, the concrete inside the specimen is compressed, the PVC pipe outside is pulled, and the load is shared by deformation coupling. The stress state of concrete changes from uniaxial compression to triaxial compression, the overall bearing capacity of the specimen is significantly improved, and the spring accumulates more elastic potential energy. However, the PVC pipe can only provide small tensile deformation before failure, and the energy consumption level of the specimen has not been effectively improved under the condition of high energy accumulation, resulting in a more intense burst of the specimen, as shown in Figures 4(e) and 4(f).

In condition 5, once the PVC material was pulled off, it will lose effect immediately, which is a brittle failure. In conditions 6 and 7, the tensile strength and ductility of the surrounding wrapping material were strengthened. Under the constraint of iron wire, the specimen was damaged step by step (Table 2). The PVC pipe was first locally damaged but still constrained by the iron wire, the spring bounced back part, the load decreased, the top expanded, and then the iron wire broke, and the specimen burst after a small increase in load. The expansion phenomenon significantly increases the energy dissipation capacity of the specimen. Although the burst phenomenon cannot be prevented due to the limited strength and ductility of the iron wire, the burst strength of the specimen is significantly weakened, as shown in Figure 4(g). In condition 7, the high ductility of the rubber material successfully prevented the fragments from flying

Table 2: Summary of test results.

Condition	Failure characteristics	State of specimen	Ultimate strength (MPa)
1	Static, shear failure	The fragments were large and uneven, leaving obvious conical residues at the top and bottom of the specimen.	12.5
2	Static, shear failure		15
3	Static to burst	The concrete was broken and flew out, the farthest distance was 1.7 m.	12
4	Static to burst	The concrete was broken and flew out, the farthest distance was 1.9 m.	13.8
5	Static to burst	The specimen burst violently, the fragment flew out 3 m, and the concrete had broken to the gravel degree.	20
6	Static to micro-motion expansion to burst	When the loading pressure reached 25 MPa, the concrete on the top of the specimen was slowly crushed, spring bounced back, which led to the axial compression deformation and radial dilation on the top of the specimen. The specimen came back to a stable state after the loading decreased to 12 MPa. When the loading continually pressed on the specimen, the iron wire ring broke and loosed, and the specimen burst violently without a significant increase in loading.	25
7	Static to micro-motion expansion to large deformation	The burst was finally been prevented under the confinement of rubber, the specimen recovered stable after large expansion deformation, and the pressure decreased to 2 MPa. A continued loading was performed, but the specimen did not present any signs of destruction even the loading reached the jacking range.	>60

(a) (b) (c) (d) (e) (f)

Figure 4: Continued.

(g)

(h)

Figure 4: Failure characteristics of concrete specimens under different experimental conditions: (a) condition 1, (b) condition 2, (c) condition 3, (d) condition 4, (e) C-1 specimen, (f) PVC pipe under condition 5, (g) C-2 specimen, and (h) C-3 specimen.

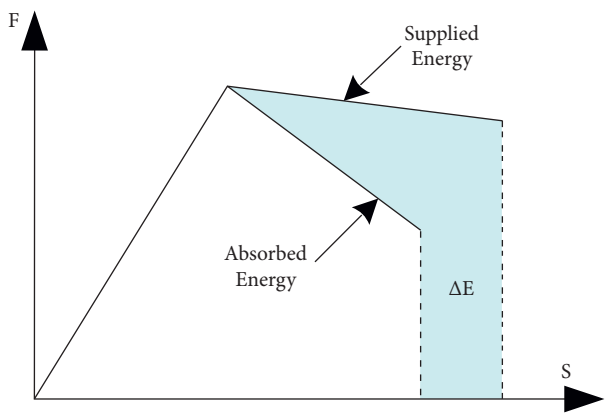

Figure 5: Comparison of loading energy and specimen energy consumption.

out, and the specimen changed from brittle failure to ductile failure. After the internal fragments were compacted, the overall strength of the specimen was higher, as shown in Figure 4(h).

2.5. Analysis on the Rockburst Control Mechanism. Based on the experiment, the conditions for inducing rockburst were revealed, and the control mechanism of rockburst was discussed.

2.5.1. Brittle Material is a Necessary Condition for Rockburst. The rock mass where rockburst occurs must be a brittle rock mass. No matter whether the rock mass is soft or hard, or whether it belongs to a strain hardening material or strain hardening-softening material, as long as its stress-strain curve is finally mutated, as shown in Figure 6, it can be defined as a generalized brittle material, and there is the possibility of rockburst, which is independent of its strength.

2.5.2. Adequate Energy is a Sufficient Condition for Rockburst. From the nonenergy storage uniaxial compression test, it can be seen that when the material is damaged, if there is no energy supplement, only static failure occurs in the specimen. However, in the uniaxial compression test of energy storage, when the damage occurs, there is also excess external energy acting on the material, and rockburst will occur. As long as the external load provides enough energy, such as the use of blasting means to recharge energy, even if the soft rock mass can burst, so under the condition of sufficient energy will produce rockburst, sufficient energy is a sufficient condition for rockburst.

2.5.3. Rockburst and Large Deformation Can Be Transformed Into Each Other. Rockburst and large deformation are essentially two different forms of surrounding rock under high energy conditions. In high energy environment, for brittle rock mass, the stiffness of the rock mass is large, the deformation during failure is small, and the absorbed energy is limited. The remaining energy is released in the form of rock mass disintegration and separation from the parent rock, namely, rockburst. For the soft rock mass, the stiffness of the rock mass is small, the plastic flow occurs when the rock mass is destroyed, and the stress redistribution shifts to the depth. The rock mass can absorb the energy given by the

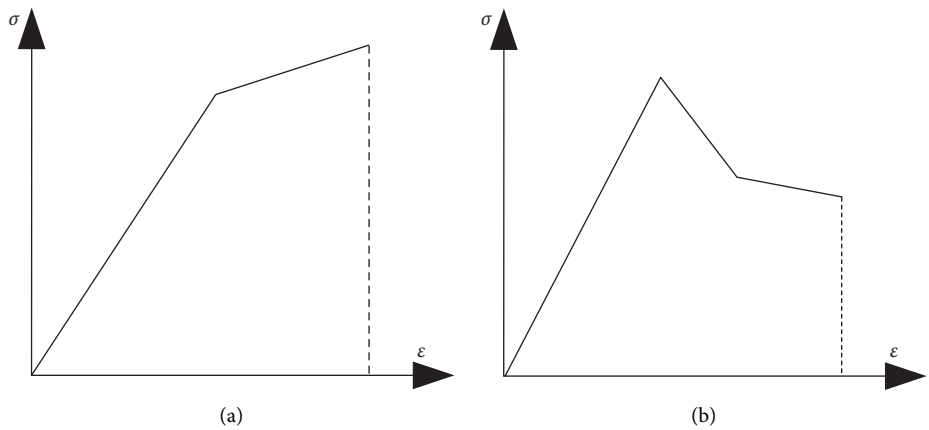

Figure 6: Stress-strain curves of generalized brittle materials: (a) strain hardening material and (b) strain softening material.

environment with large plastic deformation, which is characterized by large deformation.

In the energy storage compression test of concrete specimens confined by iron wire and PVC pipe, the specimen was damaged step by step. In the first step, the specimen showed an expansion phenomenon, and the specimen after large deformation remained stable. After continuing energy storage loading, the broken specimen under iron wire constraint was insufficient to fully absorb the energy accumulated by the system, and the ductile failure was transformed into brittle failure, that is, large deformation was transformed into rockburst. However, after the rubber was wrapped around the specimen, the concrete with brittle failure first did not fly out, but was constrained by the rubber, showing the expansion phenomenon, indicating that the energy accumulated by the system was absorbed by the broken specimen wrapped with rubber, and the brittle failure was transformed into ductile failure, and the rockburst was transformed into large deformation.

2.5.4. Exploring Energy-Absorbing Supporting Structure. In practical engineering, the occurrence of rockburst is inevitable when the necessary and sufficient conditions of rockburst are satisfied, but measures can be taken to prevent the dynamic flight of broken rock mass. Therefore, it is necessary to explore and develop the shock-resistant and energy-absorbing supporting structure and construction methods, such as the initial supporting structure with high compression and high late strength, and the structure with large deformation capacity under certain supporting resistance. The stress-strain relationship is shown in Figure 7. When a rockburst occurs, the kinetic energy of the broken rock mass can be fully absorbed, and the flying out of the broken rock mass can be effectively prevented. When a serious rockburst occurs, the structure does not collapse, and the medium and slight rockburst does not affect the normal construction, so as to avoid casualties, machine damage, and rework accidents.

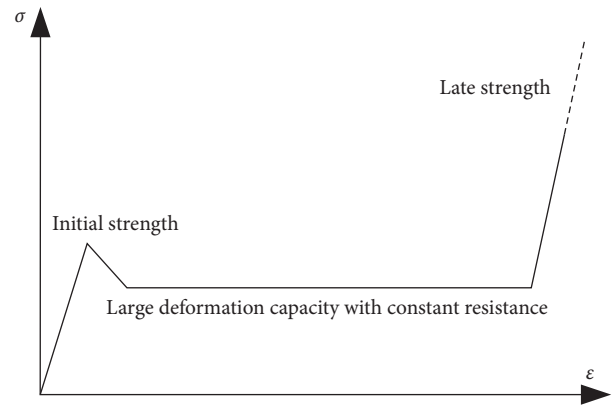

Figure 7: Stress-strain curve of energy-absorbing structure.

3. Combined Energy Absorption Support System for Rockburst Control

In the geological environment of high ground stress, the energy supply is sufficient, and the occurrence of rockburst is inevitable, but the disaster can be reduced or eliminated by measures. The rockburst control technology aims to use high energy absorption support to convert rockburst into large deformation and achieve the purpose of rockburst-expansion-static and realize rockburst-expansion-rest through energy absorption and then dissipation. The key to controlling rockburst is to absorb the kinetic energy of rockburst, which requires that the supporting structure to be high strength and large deformation. Therefore, this study proposed an energy absorption system composed of steel frames and steel pipes. The steel frame adopts the concrete-filled steel tube composite structure, giving full play to the compressive properties of concrete and the ductility of the steel pipe, greatly improving the support strength of the structure. The hollow circular steel pipe is mainly used in steel pipe, and the compressibility of steel pipe is used to absorb energy. The combination of the two can not only absorb the kinetic energy generated by the rockburst but also bear the weight of the rockfall.

3.1. Design of Combined Energy Absorption Support System. The combined energy absorption system of steel frame and steel pipe uses the concrete-filled steel tube structure instead of the original steel arch. The basic principle of concrete-filled steel tube is divided into two parts: (1) the core concrete is restrained by the steel tube, which makes the core concrete in a three-dimensional compression state, so as to improve the compressive strength and compressive deformation ability of the core concrete. (2) Since the concrete itself supports the steel tube, the stability of the steel tube is improved. Compared with the steel arch, the concrete-filled steel tube is more stable and has greater bearing capacity. In addition, the steel tube itself is a kind of mold that can withstand lateral pressure, which eliminates the process of supporting and removing the mold when pouring concrete and allows it to be used in advanced pumping concrete technology.

The action of steel pipe is to absorb the kinetic energy produced by rockburst through compression deformation. As shown in Figure 8, the steel pipes are arranged in a certain interval along the arch ring and are nested along the tunnel axis. These steel pipes are arranged in areas where rockburst may occur. Once the rockburst occurs, the rockfall first impacts the steel pipe, and the steel pipe is compressed and deformed to absorb kinetic energy. The pressure on the steel pipe increases gradually. When the yield stress of the steel frame is reached, if there is still kinetic energy, the steel frame will deform and absorb the remaining kinetic energy.

The key points of the control technology are (1) in order to maximize the energy absorption level of the hollow steel pipe and absorb the kinetic energy as much as possible, the steel frame only bears the weight of falling rock. (2) When the energy absorption capacity of the steel pipe reaches the limit, the remaining kinetic energy should be absorbed by the deformation capacity of the steel frame, while ensuring that the steel frame cannot be unstable.

3.2. Energy Absorption Effect of Steel Pipe. The Q235 B hot rolled seamless steel pipe with outer diameter $D = 108$ mm, wall thickness $t = 5$ mm, and length = 200 mm was selected, the steel plate was welded on the side of the steel pipe, and the static compression test was carried out on the press. The specimen is shown in Figure 9.

The compression load-deformation curve of the steel pipe is shown in Figure 10. The test results show that the compression deformation of steel pipe is mainly divided into four stages. The first stage is the elastic deformation stage, and the pressure increases with deformation. The second stage is the plastic constant resistance deformation stage. There is an initial peak in the steel pipe, but the initial peak is very close to the constant resistance value. The plastic deformation stage can be ignored, and the pressure is constant with the deformation. The third stage is the plastic deformation stage, and the pressure increases slowly with deformation. The fourth stage is the compaction deformation stage, and the pressure increases sharply with deformation.

The second stage of compression deformation of steel pipe is the main stage of deformation. The steel pipe undergoes continuous large-stroke deformation under constant pressure, which meets the requirements of energy absorption structure controlled by rockburst. The average effective energy absorption stroke is 80.4 mm, the constant resistance value is 82.3 kN, and the static energy absorption level per linear meter is 33.1 kJ.

3.3. Impact Numerical Test of the Energy Absorption System. In order to study the impact resistance and energy absorption capacity of steel frame-steel pipe composite system under impact load, the paper uses the finite element dynamic explicit analysis method to carry out the numerical model experiment.

3.3.1. Material Constitutive Relationship

(1) Steel Tube. The nonlinear behavior of the steel tube is modeled adopting the bilinear model, as shown in Figure 11. Material parameters are shown in Table 3.

The hardening behavior:

$$\sigma = \sigma_0 + \beta E_p \varepsilon_p^{ef}, \tag{1}$$

where σ_0 is the static yield strength of steel; β is the hardening parameter and the kinematic hardening is adopted in this analysis, $\beta = 0$; E_p is the plastic hardening modulus, and $E_p = E_t E/(E - E_t)$, ε_p^{ef} is the ffective plastic strain.

(2) Core Concrete. The core concrete is in a three-dimensional compression state under the constraint of the steel tube. Han et al. [21] put forward a stress-strain relationship of core concrete based on the uniaxial compressive strength of the concrete and the constraint effect of steel tube by summarizing the test results of concrete-filled steel tube axial compression specimens, as shown in Figure 12.

When $\varepsilon \le \varepsilon_0$,

$$\sigma = \sigma_0 \left[2\frac{\varepsilon}{\varepsilon_0} - \left(\frac{\varepsilon}{\varepsilon_0}\right)^2 \right]. \tag{2}$$

When $\varepsilon > \varepsilon_0$,

$$\sigma = \begin{cases} \sigma_0 (1 - q) + \sigma_0 q \left(\dfrac{\varepsilon}{\varepsilon_0}\right)^{0.1\xi}, & \xi \ge 1.12 \\ \sigma_0 \left(\dfrac{\varepsilon}{\varepsilon_0}\right) \dfrac{1}{\beta(\varepsilon/\varepsilon_0 - 1)^2 + \varepsilon/\varepsilon_0}, & \xi < 1.12 \end{cases}, \tag{3}$$

where $\sigma_0 = f_c[1 + (24/f_c)^{0.45}(-0.045\xi^2 + 0.4\xi)]$

$$\varepsilon_0 = 1300 + 12.5 f_c + \left[1400 + 800\left(\frac{f_c}{24} - 1\right) \right] \xi^{0.2} (\mu\varepsilon),$$

$$q = \frac{\xi^{0.745}}{2 + \xi}, \tag{4}$$

$$\beta = \left(2.36 \times 10^{-5}\right)^{[0.25 + (\xi - 0.5)^7]} f_c{}^2 \times 3.51 \times 10^{-4},$$

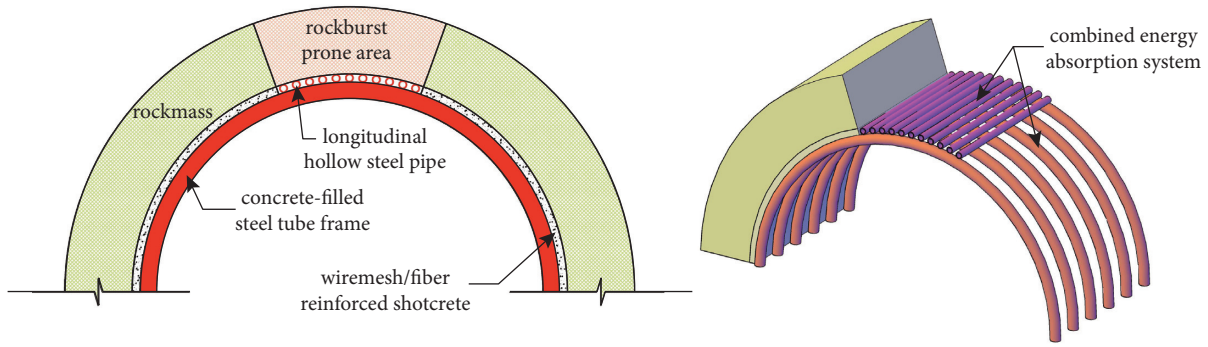

Figure 8: Combined energy absorption structure of steel frame and steel pipe.

Figure 9: Specimen for compression test of steel tube.

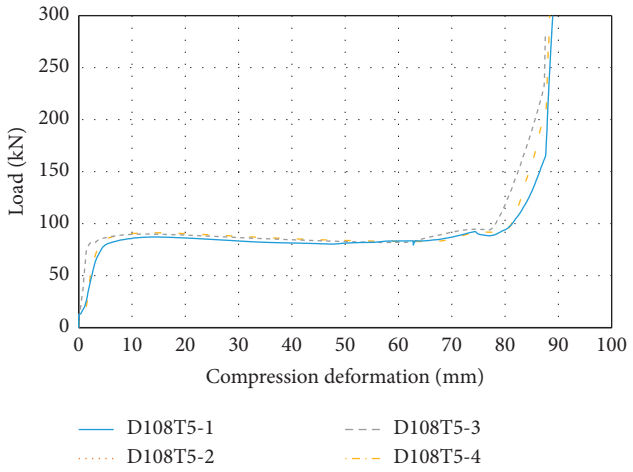

Figure 10: Compression test results of steel pipe.

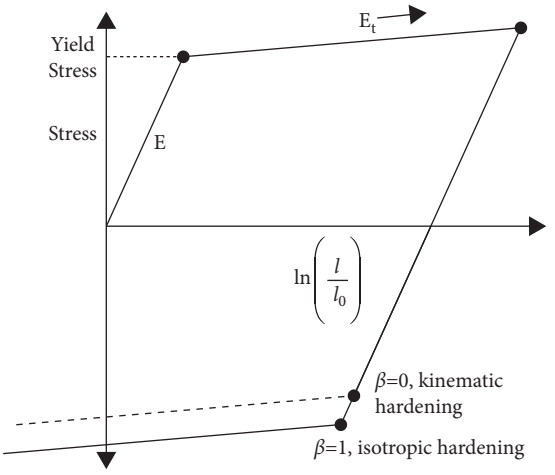

Figure 11: Stress-strain relationship of steel.

where f_c is the axial compressive strength of the concrete cylinder and ξ is the constraint effect coefficient, also known as hoop coefficient:

$$\xi = \frac{A_s f_y}{A_c f_{ck}}, \tag{5}$$

where A_s and A_c are the cross-sectional area of steel and concrete; f_y is the yield limit of steel; and f_{ck} is the standard value of axial compressive strength of concrete.

(3) Dynamic Magnification. The dynamic magnification factor of steel tube is calculated by Cowper Symonds model [22]:

$$\frac{f_{yd}}{f_{ys}} = 1 + \left(\frac{\dot{\varepsilon}}{D}\right)^{1/p}, \tag{6}$$

where f_{yd} and f_{ys} are dynamic and static yield strength of steel tube; $\dot{\varepsilon}$ is the strain rate; and D and p are material

Table 3: Steel material parameters.

Material type	Density (kg·m^{-3})	Yield strength f_y (MPa)	Elastic modulus E (GPa)	Tangent modulus E_t (GPa)	Poisson ratio
Q235	7850	235	200	1.18	0.3
Q345	7850	345	200	1.18	0.3

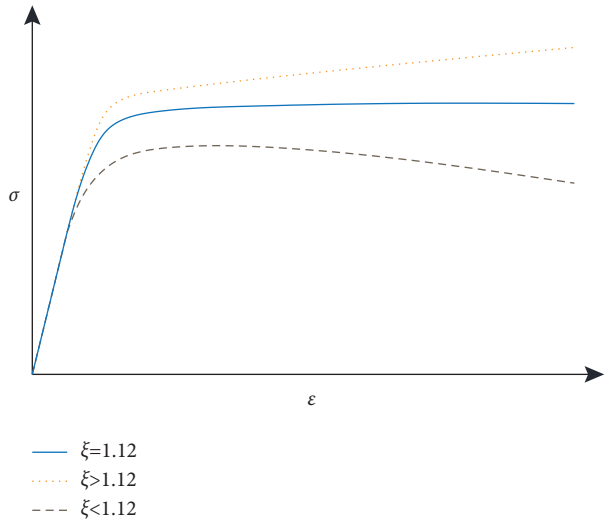

Figure 12: Stress-strain relationship of core concrete.

constants, according to the Cowper-Symonds model D and p of various metals, $D = 40$ and $p = 5$.

According to the European FIB MODEL CODE specification [23], the dynamic magnification factor of concrete is as follows:

$$\frac{f_{cd}}{f_{cs}} = \begin{cases} \left(\dot{\varepsilon_c}/\dot{\varepsilon_{c0}}\right)^{0.014}, & \dot{\varepsilon_c} \le 30s^{-1} \\ 0.012\left(\dot{\varepsilon_c}/\dot{\varepsilon_{c0}}\right)^{1/3}, & \dot{\varepsilon_c} > 30s^{-1} \end{cases}, \tag{7}$$

where f_{cd} and f_{cs} are dynamic and static axial compressive strength of concrete; $\dot{\varepsilon_c}$ is the strain rate of concrete; and $\dot{\varepsilon_{c0}} = 30 \times 10^{-6}s^{-1}$ is the reference strain rate.

Dynamic hoop coefficient ξ_d:

$$\xi_d = \frac{A_s f_{yd}}{A_c f_{cd}}. \tag{8}$$

By replacing f_c and ξ in equation (2) to (4) with f_{cd} and ξ_d, respectively, the dynamic magnified stress-strain relationship of core concrete is obtained.

3.3.2. Introduction of Calculation Model. Taking a typical TBM tunnel in high geo-stress environment as the prototype, the rockburst disaster controlling effect of the combined energy absorption system was numerically tested through Abaqus dynamic explicit analysis. A semi-circular arch tunnel model, shown in Figure 13, is used. The tunnel is 8.0 m in diameter and 2.5 m in length, and the thickness of the surrounding rock is 0.5 m. The center distance of each concrete-filled steel tube arch is 0.5 m. The longitudinal hollow small steel pipes are distributed along the concrete-filled steel tube arch with a spacing of 0.14 m below the burst-prone area. The rockburst was simulated by vertical impacting 4 pieces of rockfall on the support system in the burst-prone area. The rockfall pieces are within the range of 30° from the vault to the left and right sides of the arch waist and have a height of 0.5 m. The total volume of the rockfall pieces is 4.73 m^3. According to St-Pierre et al. [24], during a rock burst of moderate to major severity, the rejected rock mass can reach velocities between 3 and 10 m/s with corresponding energy levels varying from 10 to 50 kJ/m^2. The impact velocity is set as 10 m/s to simulate a strong rockburst, and the density of the rockmass is 2500 kg/m^3. Then the total impact energy is equal to $0.5 * 4.73 * 2500 * 10\hat{}2 = 591.3$ kJ, and the impact energy density on the support is $591.3/2.5/(\pi/6 * 8) = 56.5$ kJ/m^2.

The concrete, steel tube, and hollow steel pipe adopt a solid unit (C3D8R). Along the axis direction of the concrete-filled steel pipe arc arch, the element size is 50 mm when there are hollow steel pipes distributed and 100 mm when the absence of steel pipes. In the concrete-filled steel tube, the contact between the steel tube and the concrete is restrained by a tie, and the contact between hollow steel pipes and steel frame is also restrained by a tie to simulate welding. The steel tube frames are tied together with surrounding rock at each arch foot. And a general hard contact is applied in other places of the model. The bottom and lateral boundaries of the surrounding rock are fixed during the simulation. The surrounding rock is modeled by elastic material with the young's modulus of 50 GPa and the Poisson ratio of 0.25. The gravity acceleration is 9.8 m/s^2.

In the concrete-filled steel tube frame, the outer diameter of the steel tubes is 150 mm and the wall thickness is 9 mm, the material of steel tubes is Q345, and the strength grade of concrete is C40. In order to evaluate the rockburst control effect of different types of composite structure, three support conditions under the rockfall impact were calculated, as shown in Table 4. There are no steel pipes in condition 1, and there are 29 steel pipes arranged in equal spacing within the range of 60°. The outer diameter of the steel pipes is 50 mm, and the wall thickness is 1 mm. The material of the steel pipes is Q235 in condition 2 while Q345 in condition 3.

3.3.3. Result Analysis. Based on the evolution of structural impact force, vertical displacement of structural vault, distribution of plastic zone, and energy absorption with time, this paper compared and analyzed the structural stability and rockburst control effect under three working conditions.

(1) Impact Force Variation Characteristics. It can be seen from Figure 14 that the trend of time-history curves in the three cases is the same, and the time to reach the peak of impact force is $t = 0.008$ s. The peak load of impact force was 511.4 kN (without hollow steel pipes), 449.3 kN (Q235), and 492.0 kN (Q345), respectively. Under the working condition

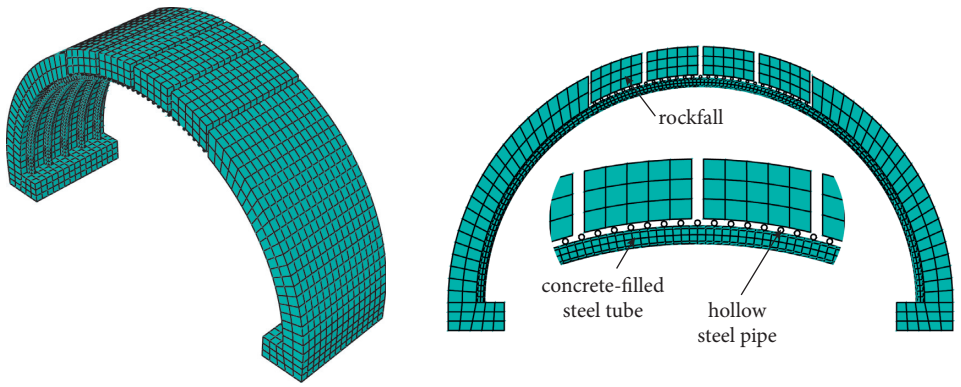

Figure 13: Numerical model.

Table 4: Calculated working conditions.

No.	Working condition	Steel pipe size $D * t$ (mm * mm)
1	No hollow steel pipes	—
2	Q235 steel pipes	50 * 1
3	Q345 steel pipes	50 * 1

of hollow steel pipe, the peak load was reduced by 12.1% (Q235) and 3.8% (Q345), respectively, indicating that hollow steel pipe materials have a certain buffer effect on the impact load, and with the increase of the yield strength of hollow steel pipe, the structural stiffness increases and the impact resistance decreases. Then the subsequent curves gradually attenuated to zero, and the time when the impact force attenuated to zero was $t = 0.028$ s, $t = 0.032$ s, and $t = 0.030$ s, respectively. However, under the working conditions of no hollow steel pipe and Q345, there were rebound in different amplitudes during the decline of the impact force curve, and the structure without hollow steel pipes was more obvious, which was easier to cause secondary damage to the support structure. This situation did not occur under Q235 working condition, which avoided multiple impacts on the support structure.

(2) Vertical Displacement Characteristics of the Vault. It can be seen from Figure 15 that at the beginning of the impact, the displacement growth rate of the structure without hollow steel pipes was significantly greater than that with hollow steel pipes, while the displacement change difference between the two working conditions with steel pipes was small. When $t = 0.016$ s, the vertical displacement of the three working conditions reached the maximum, which were 76.9 mm (without hollow steel pipes), 68.6 mm (Q235), and 71.5 mm (Q345). The two working conditions with hollow steel pipes decreased by 10.8% (Q235) and 7.0% (Q345), respectively. Due to the difference in material stiffness, the vertical displacement of the vault under Q235 steel condition was 2.9 mm smaller than that under Q345 steel condition. After reaching the maximum vertical displacement, the structure began to rebound. When $t = 0.036$ s, the rebound reached the minimum value under the condition of no hollow steel pipe and Q345 steel, which were 21.9 mm and 16.9 mm, respectively. When $t = 0.040$ s, the rebound under

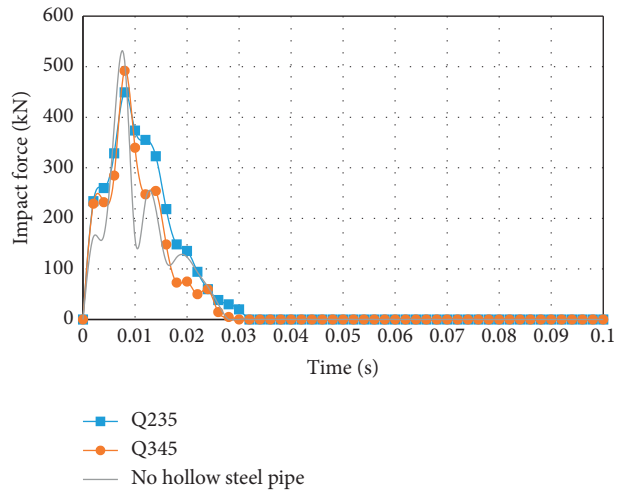

Figure 14: Impact force time history of supporting structure under different working conditions.

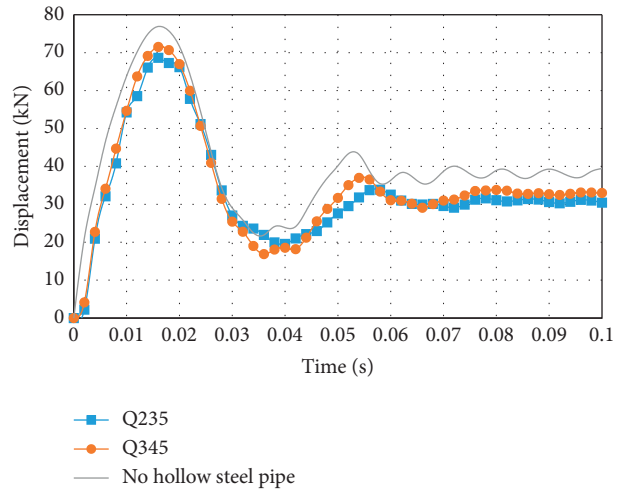

Figure 15: Vertical displacement changes of the vaults of different support structures.

the working condition of Q235 steel reached the minimum value of 19.5 mm. In terms of the final vertical displacement, the working condition of no hollow steel pipe was 39.4 mm,

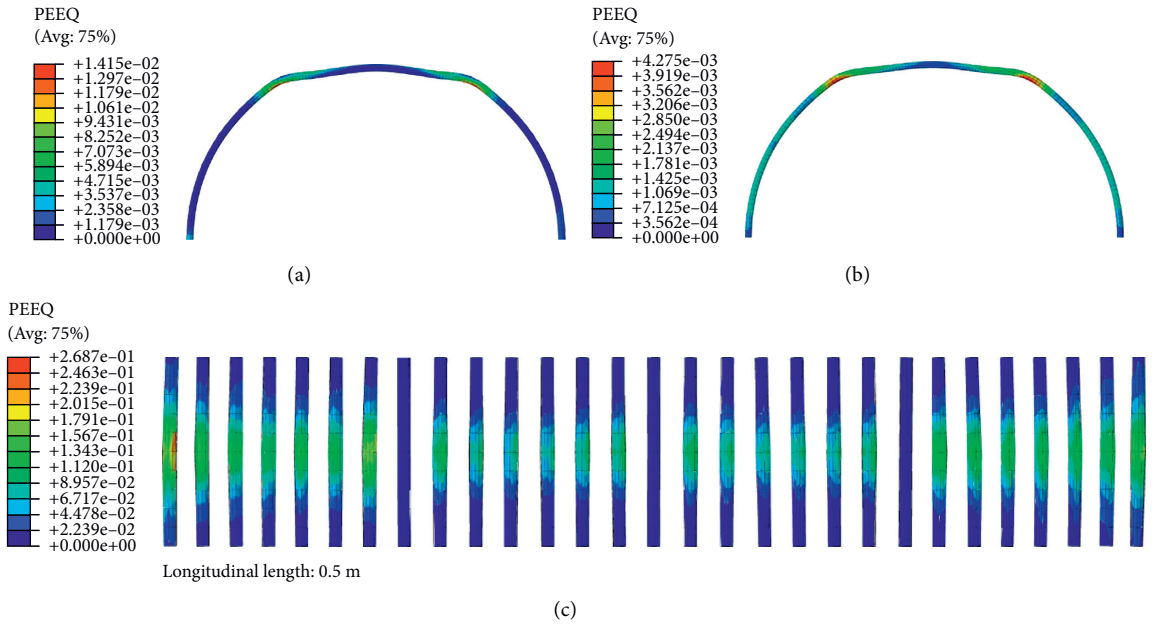

Figure 16: Plastic zone of the energy-absorbing structure under Q235 Condition. (a) Plastic zone of steel frame, (b) plastic zone of concrete, (c) plastic zone of hollow steel pipes.

the working condition of Q235 steel was 30.4 mm, and the working condition of Q345 steel was 33.0 mm.

In addition, due to the obvious vibration of the structure without hollow steel pipes, the stability time of the final displacement is obviously longer than that of the two conditions with hollow steel pipes. The higher the strength of the hollow steel tube is, the larger the vibration amplitude of the structure caused by the impact is, and the larger the final vertical displacement is.

(3) Distribution Characteristics of Plastic Zone. It can be seen from Figures 16 and 17 that due to the difference in the yield strength of the hollow steel pipe material, the higher the yield strength of the hollow steel pipes is, the greater the plastic strain value of the steel arch and the concrete is. This is due to the decrease of the cushioning energy absorption of the hollow steel pipes, resulting in the increase of the plastic strain and the distribution of the plastic zone of the lower structure. The maximum plastic strains of steel frame and concrete appeared at the lower edge of the rockfall.

3.4. Energy Absorption Effect. The energy conversion is an important index to measure the absorbing kinetic energy performance of concrete-filled steel tube arch. In the finite element dynamic explicit analysis, the energy output is also an important part. The mathematical expressions of energy conversion and balance of the model are as follows:

$$E_I + E_V + E_{FD} + E_K - E_W = E_{TOTAL}, \tag{9}$$

where E_I is the internal energy of the system; E_V is the viscous dissipation energy of the system; E_{FD} is the friction dissipation energy of the system; E_K is the kinetic energy of the system; E_W is the external work, in this paper, gravity works; and E_{TOTAL} is the total energy of the system, a constant. The internal energy E_I of the system consists of the following energy components:

$$E_I = E_{SE} + E_{PD} + E_{CD} + E_{AE}, \tag{10}$$

where E_{SE} is recoverable elastic strain energy; E_{PD} is the dissipation energy of inelastic strain, and it is the plastic strain energy in this paper; E_{CD} is creep energy, which refers to the energy dissipation caused by damping, damping is not considered in this paper, so the zero value is maintained; and E_{AE} is artificial strain energy, also known as pseudo strain energy and sand leakage energy. General explicit analysis requires strict control of the proportion of artificial strain energy in the internal energy. In engineering, if the artificial strain energy accounts for less than 5% of the internal energy, the calculation results are reliable. After calculation, the artificial strain energy in this paper accounts for 3.9% of the internal energy, less than 5%, so the calculation result is reliable.

It can be seen from Figure 18 that under the same impact of kinetic energy, the internal energy conversion rate under the condition without hollow steel pipes was greater than that under the other two conditions with hollow steel pipes. This is because the hollow steel pipe can be regarded as a buffer structure, and the structure without hollow steel pipes directly contacts with the concrete-filled steel tube with poor energy dissipation effect, so the energy conversion is faster. In addition, the existence of hollow steel pipes can absorb a part of the impact kinetic energy, so from the aspect of kinetic energy transforming into structural internal energy, the working condition with hollow steel pipes is better than that without hollow steel pipes. Taking the efficiency of the impact energy conversion into the final internal energy as the energy absorption index, the overall energy absorption rate of the structure without hollow steel pipes was 64.8%,

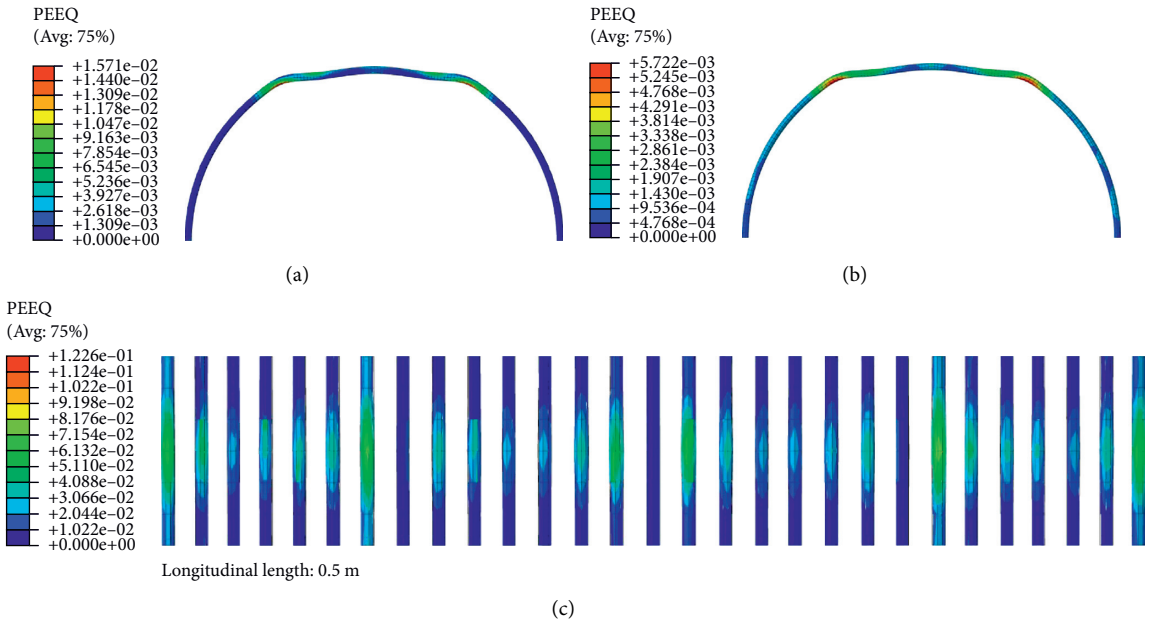

Figure 17: Plastic zone of energy-absorbing structure under Q345 Condition. (a) Plastic zone of steel frame, (b) plastic zone of concrete, (c) plastic zone of hollow steel pipes.

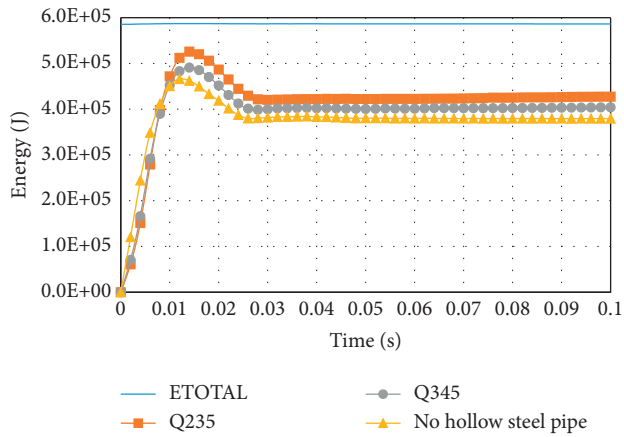

Figure 18: Time history variation of internal energy of the structure under different working conditions.

the overall energy absorption rate of the structure with Q235 hollow steel pipes was 73.0%, and the overall energy absorption rate of the structure with Q345 hollow steel pipes was 69.0%. It can be seen that the combined energy absorption system with small stiffness has the best energy absorption effect for the impact effect.

To sum up, the combined energy absorption support can withstand the strong rockburst impact. The hollow steel pipes effectively reduced the impact force and vertical displacement, and the smaller the strength of the hollow steel pipe is, the smaller the impact force and the final displacement is. Compared to the current widely used energy-absorbing bolt system, the combined energy absorption support system adopts flexible pipes to reduce the impact intensity and stiff frames to restrict the deformation and stabilize the entire system. The rockburst disaster can be controlled after a relatively small expansion deformation, which is very important for tunnel clearance management. At present, the combined energy absorption structure has been preliminarily applied in the high horizontal geo-stress sections in Yangshan tunnel of Menghua railway. The vault of Yangshan tunnel was cracked with a small deformation after conventional support, as shown in Figure 19(a), and sporadic sound of rock fracture occurred in the depth of surrounding rock. Since the elastic deformation energy density was small and the work worn for destruction fracturing kept increasing, the energy balance [25] in the surrounding rock matched the fifth grade of the classification, which means that countermeasures should be taken to deal with the possible occurrence of rockburst. According to the field situation, a combined energy absorption structure was designed and applied in the weak

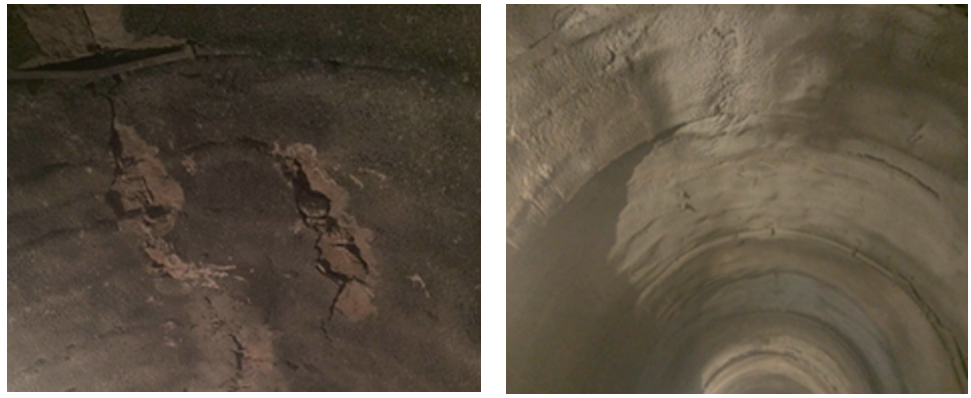

(a) (b)

Figure 19: Effect comparison of conventional support and combined energy absorption structure. (a) Cracking of surrounding rock under conventional support. (b) The supporting effect of combined energy absorption structure.

area of the surrounding rock. Through the field test, the combined energy absorption structure effectively controlled the occurrence of cracking, as shown in Figure 19(b), which further confirmed the better energy absorption effect of the combined energy absorption structure.

4. Conclusions

Through the originally developed uniaxial energy storage loading device, uniaxial energy storage and nonenergy storage experiments of concrete specimens under different constraints were carried out, and the control mechanism of rockburst was studied. Based on the experimental results, a combined energy absorption support system for rockburst control in tunnelling was proposed. The effectiveness of the support was verified by numerical simulation. The main conclusions are as follows:

(1) The loading tests' results show that specimens with low confinements burst violently under energy storage loading, while the burst was finally restrained by high confinements and transformed into large expansion deformation. The occurrence of rockburst is inevitable under the sufficient and necessary conditions of brittle materials and sufficient energy, but measures can be taken to control rockburst to avoid casualties, machine damage, and rework accidents. The concept of gradually consuming kinetic energy by adopting shock-resistant and energy-absorbing structures to control the disaster after the rockburst was proposed.

(2) A combined energy absorption support system based on concrete-filled steel tubes and hollow steel pipes was proposed to control rockburst disasters. The concrete-filled steel tube frames act as the strong confinement part in the system to provide strength and stability. The longitudinal hollow steel pipes distributed along the frame arch under the burst-prone area act as the energy-absorbing part to buffer the rockburst impact.

(3) The numerical analysis on the dynamic response of the support under strong rockburst impact shows that the system can not only absorb rockburst kinetic energy efficiently but also have good impact resistance, which can meet the high-level rockburst dynamic impact support. The material stiffness of the hollow steel pipes has a great influence on the rockburst control. The peak force impacted on the frames was reduced by 12.1% (Q235) and 3.8% (Q345), respectively, and the final displacement was reduced by 10.8% (Q235) and 7.0% (Q345), respectively. The steel pipe material with appropriate stiffness should be selected according to the site rockburst disaster, in order to obtain the best rockburst control effect.

Data Availability

The data used to support the findings of this study are included within the article.

Conflicts of Interest

The authors declare that they have no conflicts of interest.

References

[1] A. Kidybiński, "Bursting liability indices of coal," *International Journal of Rock Mechanics and Mining Science & Geomechanics Abstracts*, vol. 18, no. 4, pp. 295–304, 1981.

[2] Y. S. Pan, M. T. Zhang, and L. G. Wang, "Study on rockburst by equivalent material simulation tests," *Chinese Journal of Geotechnical Engineering*, vol. 4, pp. 49–56, 1997.

[3] Y. S. Pan, M. T. Zhang, and G. Z. Li, "Analysis on circular chamber rockburst by dynamic stability criterion," *Chinese Journal of Geotechnical Engineering*, vol. 5, pp. 59–66, 1993.

[4] Y. N. Xu, W. S. Xu, Y. H. Wang, and L. G. Tham, "Simulation testing and mechanism studies on rockburst," *Chinese Journal of Rock Mechanics and Engineering*, vol. 10, pp. 1462–1466, 2002.

[5] A. Golshani, Y. Okui, M. Oda, and T. Takemura, "A micromechanical model for brittle failure of rock and its

relation to crack growth observed in triaxial compression tests of granite," *Mechanics of Materials*, vol. 38, no. 4, pp. 287–303, 2006.

[6] H. Zhou, R. C. Xu, and J. J. Lu, "Experimental study of instability destruction and crack propagation characteristics of slab failure model specimen," *Rock and Soil Mechanics*, vol. 36, no. 2, pp. 1–11, 2015.

[7] M. C. He, J. L. Miao, and D. J. Li, "Experimental study on rockburst processes of granite specimen at great depth," *Chinese Journal of Rock Mechanics and Engineering*, vol. 5, pp. 865–876, 2007.

[8] F. Meng, H. Zhou, Z. Wang et al., "Experimental study on the prediction of rockburst hazards induced by dynamic structural plane shearing in deeply buried hard rock tunnels," *International Journal of Rock Mechanics and Mining Sciences*, vol. 86, pp. 210–223, 2016.

[9] R. Shirani Faradonbeh, A. Taheri, L. Ribeiro E Sousa, and M. Karakus, "Rockburst assessment in deep geotechnical conditions using true-triaxial tests and data-driven approaches," *International Journal of Rock Mechanics and Mining Sciences*, vol. 128, 2020.

[10] W. D. Liu, J. Q. Li, and L. Li, "Review of research stutus on rockburst," *Gold*, vol. 31, no. 1, pp. 26–28, 2010.

[11] L. Guo, X. B. Li, and X. M. Yan, "Research progress and development trend of rockburst," *Mining Technology*, no. 1, pp. 16–20, 2006.

[12] M. T. Zhang, "Instability theory and methematical model for coal/rockbursts," *Chinese Journal of Rock Mechanics and Engineering*, vol. 3, pp. 197–204, 1987.

[13] E. Hoek and E. T. Brown, *Underground Excavations in Rock*, Institution of Mining and Metallurgy, London, 1980.

[14] Y. A. Tan, "The mechanism research of rockburst," *Hydrogeological and Engineering Geology*, no. 1, pp. 34–38, 1989.

[15] L. S. Xu, "Research of rockburst formation condition in underground engineering," *Journal of Chongqing Jianzhu University*, no. 3, pp. 31–34, 2005.

[16] Q. H. Qian, "Challenges faced by underground projects construction safety and countermeasures," *Chinese Journal of Rock Mechanics and Engineering*, vol. 31, no. 10, pp. 1945–1956, 2012.

[17] X. T. Feng, B. R. Chen, and C. Q. Zhang, *Mechanism, Warning and Dynamic Control of Rockburst Development Processes*, Science Press, Beijing, 2013.

[18] B. Wang, X. B. Li, and C. D. Ma, "Principle and preliminary application of combined static-dynamic support to rockburst disaster controlling," *Chinese Journal of Rock Mechanics and Engineering*, vol. 33, no. 6, pp. 1169–1178, 2014.

[19] J. J. Zhang and B. J. Fu, "Rockburst and its criteria and control," *Chinese Journal of Rock Mechanics and Engineering*, no. 10, pp. 2034–2042, 2008.

[20] X. F. Lv and Y. S. Pan, "Theoretical analysis and experimental research on rockburst prevention mechanism of rigid-flexible-rigid supporting structure," *Chinese Journal of Rock Mechanics and Engineering*, vol. 31, no. 1, pp. 52–59, 2012.

[21] L. H. Han and J. B. Feng, "Constitutive relations of concrete and its applications in the entegral analysis of concrete filled steel tube," *Journal of Harbin University of Architecture and Engineering*, no. 5, pp. 26–32, 1995.

[22] N. Jones, *Structural Impact*, Cambridge University Press, New York, 1997.

[23] *Fib Model Code for Concrete Structures 2010*, Structural I F F, Lausanne. Switzerland, 2013.

[24] L. St-Pierre, F. P. Hassani, P. H. Radziszewski, and J. Ouellet, "Development of a dynamic model for a cone bolt," *International Journal of Rock Mechanics and Mining Sciences*, vol. 46, no. 1, pp. 107–114, 2009.

[25] K. Skrzypkowski, "Laboratory testing of a long expansion rock bolt support for energy-absorbing applications," *E3S Web of Conferences*, vol. 29, p. 4, 2018.